International Journal of Scientific Research in Physics and Applied Sciences
Vol.**12**, Issue.**6**, pp.**07-18**, December **2024**
E-ISSN: 2348-3423
Available online at: www.isroset.org

Research Article

Synthesis and Complex Optical Study of Chemically Synthesized Cerium Oxide Nanoparticles

Shubham Kadam[1*], Vivek Kapse[2], Kailash Nemade[3]

[1]Dept. of Physics, Prof. Ram Meghe College of Engineering and Management Amravati- 444701, Maharashtra, India
[2]Dept. of Physics, Arts, Science and Commerce College, Chikhaldara- 444807, Maharashtra, India
[3]Dept. of Physics, Indira Mahavidyalaya, Kalamb-445401, Maharashtra, India

**Corresponding Author: simplyshubs@gmail.com*

Received: 21/Oct/2024; **Accepted**: 23/Nov/2024; **Published**: 31/Dec/2024

Abstract— This research explores the influence of probe sonication on the structural, optical, and thermal characteristics of CeO_2 nanoparticles. The nanoparticles were produced through an innovative co-precipitation technique and then exposed to different sonication times (0, 15, 30, 45, and 60 minutes). The structural analysis via XRD revealed an FCC structure with particle size reduction from 29.2 nm (without sonication) to 14.6 nm (60 minutes sonication). TEM and SEM imaging confirmed the decreased aggregation and improved uniformity with longer sonication times. The optical properties, examined using UV-Vis and PL spectroscopy, showed a blue shift in both the absorption edge and emission peaks. This shift suggests the presence of quantum confinement effects and improved crystalline quality as the sonication duration increased. The optical band gap expanded which starts at 2.81 eV to 3.01 eV. Additionally, extinction coefficient, refractive index, and optical conductivity measurements showed significant changes with sonication, reflecting improved dispersion and uniformity.

Keywords— cerium oxide; probe sonication; optical study; particle size; nanoparticles; extinction coefficient

1. Introduction

Cerium dioxide (CeO_2) nanoparticles find applications in a wide array of fields, including sensing devices, biomedical equipment, energy storage systems, and memory devices, owing to their distinctive and adaptable properties. One of their most significant features is their outstanding redox capability, particularly their oxygen storage capacity, which enables the transition between Ce^{4+} and Ce^{3+} oxidation states. This characteristic makes them highly efficient in both catalysis and gas detection. The redox behavior plays a crucial role in gas detection and conversion, boosting catalytic performance, especially in automotive catalytic converters and various chemical reactions within sensing devices [1]. Moreover, the nanoscale size of CeO_2 nanoparticles results in a large surface area, which increases their reactivity by providing additional active positions for chemical interactions, thus enhancing the effectiveness of energy storage systems and catalytic processes. CeO_2 chemical stability, which helps it resist corrosion and environmental degradation, also makes it highly suitable for extended use in biomedical devices and energy storage applications [2-4]. CeO_2 nanoparticles also possess notable optical properties, such as UV absorption, making them useful in sunscreens and UV protection coatings, and they exhibit photocatalytic activity, which is beneficial for environmental cleanup and energy generation through processes like water splitting. Their biocompatibility and low toxicity are critical for biomedical usage, comprising medication delivery, imaging, and as antioxidants in healing treatments, capacity to search reactive oxygen species and defend against oxidative strain in biological systems [5-8].

Further, versatility in preparation of CeO_2 nano-sized particles, allowing for controlled shapes and sizes, enables the tailoring of properties to suit specific applications across various fields. These collective properties make CeO_2 nanoparticles highly versatile and appropriate for a wide-range of practice [9] In the literature of materials science, several studies have been reported by researchers worldwide to explore the various potential applications associated with CeO_2 nanoparticles and few of them are discussed in this section. Fudala et al explores preparation of CeO_2 nanoparticles with varying sizes and band gaps through sol-gel technique. The primary goal of the research is to determine how the concentration of precursors affects the final characteristics of CeO_2 nanoparticles. The sol-gel method was chosen because of its ease of use, affordability, and ability to create nanoparticles with specific characteristics. In this study, band gap values were found to vary between 3.2 and 3.4 eV. The capacity to regulate the dimensions and band gap of the nanoparticles offers

auspicious prospects for utilisation in domains including energy storage, sensors, and catalysis [10].

The ability of CeO_2 nanoparticles produced at room temperature using the chemical precipitation process to sense gases was examined by Oosthuizen et al. The findings showed that the CeO_2 nanoparticles have useful features for gas sensing, with defect concentrations less than 10% and typical crystallite sizes between 6 and 8 nm. Insightful information for the creation of effective gas sensing technologies is provided by this work, which emphasises the complex link between the properties of CeO_2 nanoparticles and their gas sensing abilities [11].

In order to create materials with unique characteristics, Sonawane et al. studied the synthesis of CeO_2 nanoparticles utilising sol–gel and hydrothermal techniques. Using the sol–gel and hydrothermal approaches, the band gap energies were determined to be 3 eV and 3.16 eV, respectively. Comprehensive characterisation of CeO_2 nanoparticles synthesised by hydrothermal and sol-gel processes was provided by the study, offering insightful information on their optical and structural characteristics. These revelations greatly advance our knowledge of the methods used in the creation of nanoparticles and the range of possible uses they have. [12]. An economical chemical technique for producing CeO_2 nanoparticles without the need for surfactants or additives was studied by Nimbalkar et al. This technique improved the simplicity and efficiency of synthesis by enabling it to occur at low temperatures and short reaction periods. The effect of temperatures on the physical properties including structural, morphological and chemiresistive characteristics of the produced CeO_2 nanoparticles was examined using a variety of methods. The work addresses the urgent demand for dependable and reasonably priced sensing technologies by offering insightful information on the design and optimisation of CeO_2-based gas sensors [13]. In order to create CeO_2 nanoparticles, Pathak et al. studied the use of a straightforward and affordable chemical precipitation technique. The characteristics of the synthesised metal oxide nanoparticles were investigated by means of a range of characterisation methods. This work contributes to our understanding of the possible uses of CeO_2 in a variety of sectors by providing insightful information on the chemical and structural characteristics of the particles produced via chemical precipitation [14]. In order to detect nitrogen dioxide gas, Kabure et al. focused their investigation on the creation of gas sensors employing innovative nanomaterials, such as CeO_2, NiO, and CeO_2-NiO composite. The goal of the study was to assess these nanomaterials' qualities and usefulness as NO_2 gas sensors, with a focus on low NO_2 gas concentrations and ideal operating temperatures. The researchers produced extremely crystalline nanomaterials consisting of CeO_2, NiO, and CeO_2-NiO by using a microwave-assisted sol-gel method. Considerable light is shed on the possible uses of these nanoparticles in gas sensing technologies by this work. The results highlight the potential of CeO_2, NiO, and CeO_2-NiO nanocomposites as efficient NO_2 gas sensors, especially in situations where sensitivity to low concentrations of the target gas is required [15].

A trustworthy investigation of the production of CeO_2 nanoparticles by hydrothermal and co-precipitation techniques was carried out by Pujar et al. The study highlights how well the hydrothermal approach works for producing CeO_2 nanoparticles that are specifically designed for use in biomedical applications. Characteristic peaks at 283 and 274 nm were seen in the absorption spectra, indicating that the hydrothermal and co-precipitation processes, respectively, were used to generate the CeO_2 nanoparticles. This work highlights the potential of CeO_2 nanoparticles for antibacterial therapeutics and biomedical applications by offering insightful information on their biological activity and production [16].

Ko et al. used cerium nitrate hexahydrate and coprecipitation techniques to create nanoscale CeO_2 particles. The single crystalline phase of CeO_2 in the precursor powders both before and after calcination was verified by this investigation. The crystallite size grew after 240 minutes of post-calcination at 1273 K, from 10.4 nm to 66.8 nm. The investigation also showed that when crystallite size increased, the indirect and direct band gap energies of CeO_2 decreased, going from 3.03 eV to 2.68 eV and 3.79 eV to 3.38 eV, respectively. This work highlights the optical characteristics of nanosized CeO_2 powders and the impact of crystallite size on band gap energy, offering important new insights into their production and characterisation [17].

In an effort to get around the drawbacks of high working temperatures in gas sensors, Kumar et al. looked into the production of pure and Al-doped CeO_2 nanoparticles for Room-Temperature NO_2 detection. Three times more than the virgin CeO_2, the 5% Al-doped CeO_2 responded to 25 ppm of NO_2 with an astounding 247%. The sensor demonstrated superior stability and repeatability over a 56-day period, with recovery durations of 52 s and response times of 64 s, respectively. This work opens the door to real-time gas sensors appropriate for room temperature applications by offering insights on improving gas sensing performance by Al doping [18]. Using a polyaniline-cerium dioxide nanocomposite thin film produced by in-situ self-assembly, Liu et al. created a flexible NH_3 sensor. The sensor demonstrated exceptional NH_3-sensing capabilities, including improved stability, faster recovery times, and increased responsiveness. Due to the altered PANI shape and p-n junction effect, the PANI-CeO_2 sensor continued to function even after 500 bending/extending cycles. Long-term functioning was facilitated by its stickiness and flexibility. This study represents a substantial breakthrough in flexible sensor technology for the detection of NH_3 at the trace level, with potential applications in industrial safety and environmental monitoring [19]. Li and colleagues presented a unique strategy to improve ethanol sensing: low-temperature solvothermal synthesis of CdS nanowires decorated with CeO_2 nanoparticles. The performance of CdS sensing was greatly enhanced by CeO_2 modification; in particular, the 5 at% CeO_2/CdS composite responded to 100 ppm ethanol 2.6 times more quickly than pure CdS. These composites demonstrated remarkable selectivity in addition to quick reaction and recovery times (<12 s and <3 s, respectively)

[20]. Using surfactant-mediated hydrothermal methods, Mohanta et al. present a one-step synthesis approach for SnO_2 nanoparticle–CeO_2 nanorod sensing material. This material demonstrates dual capability for low-concentration arsenic optosensing and room-temperature CO gas sensing. At room temperature, the sensor exhibits a robust reaction to CO gas, with a quick response time of 21.1 s and a recovery time of 59.6 s at a low concentration of 3 ppm. Moreover, it exhibits remarkable sensitivity at low CO gas concentrations (1 ppm), outperforming pure SnO_2 sensors by a factor of around 6.7. The oxygen vacancies and CeO_2-SnO_2 n-n heterojunction are responsible for the improved sensing characteristics. With implications for water quality evaluation and environmental monitoring, this work enhances multifunctional sensor technology [21].

Majumder et al. provide a technique that uses reversed micelles in a water-in-oil microemulsion to create mesoporous CeO_2 nanospheres with a large surface area. Compared to comparable sensors, undoped CeO_2 nanospheres exhibit better selectivity, sensitivity, and response-recovery times for low-ppm CO detection. They achieve about 52% sensitivity with a quick reaction time of 13 seconds. Temperature and gas concentration data from the sensor are analysed. The work also emphasises the affordable synthesis and manufacture of packed CO sensors, indicating the possibility of using them for environmental and industrial monitoring applications [22]. According to Tumkur et al., the extensive use of CeO_2 nanoparticles has caused their leakage into the environment, raising questions regarding potential human exposure, particularly through inhalation. Using Beas-2B cells, the cytotoxicity and biocompatibility were evaluated using MTT and Live/Dead tests. The results showed no appreciable cell death, even at higher doses. The results illustrate the safety and biocompatibility of CeO_2 nanoparticles and highlight their prospective uses in medication delivery, sunscreen, cancer treatment, biosensors, and catalytic converters [23]. Munoz et al. synthesized ceria nanoparticles via a modified polymer complex process, varying the system pH to achieve reproducible, chemically pure ceria (<100 nm) at low temperatures. UV–vis absorption and diffuse reflectance spectroscopy yielded energy values of 3.8 eV and 3.4 eV, potentially representing the energy gap. Increasing synthesis pH resulted in smaller particle sizes (10-20 nm, spheroidal shape). A proposed mechanism elucidates ceria nanoparticle formation throughout the synthesis process [24]. Pol et al. use surfactants such cetyl trimethyl ammonium bromide and sodium dodecyl sulphate in a hydroxide-mediated method to synthesise cerium oxide nanoparticles (20–100 nm). These surfactants are essential for regulating the size and form of the nanoparticles that are made from hexahydrate cerium nitrate. Moreover, the polymer polyvinyl pyrrolidine envelops cerium oxide nanoparticles. Furthermore, disc diffusion experiments are used to assess the antibacterial effectiveness of nanoceria against both Gram-positive and Gram-negative bacteria [25].

Ioannou et al. study hemocompatible ceria nanoparticles with the ability to scavenge reactive oxygen species for titanium implant coatings in order to treat bacterial invasion and inflammation that lead to implant failure. In the Ce^{+3} and Ce^{+4} oxidation states, cerium contributes to the antibacterial, antioxidant, catalytic, and reactive oxygen species-scavenging properties. CeO_2 nanoparticles are therefore particularly attractive as candidates for use as antibacterial nanofillers or nanocoatings [26]. Nyoka et al. examine the therapeutic potential of cerium oxide nanoparticles, focusing on their oxidative stress amelioration capabilities. These nanoparticles demonstrate enzyme-mimetic catalytic activity by interconverting between Ce^{3+} and Ce^{4+} species, making them effective free-radical scavengers for systemic and neurodegenerative diseases. This comprehensive analysis sheds light on the potential applications and safety considerations of cerium oxide nanoparticles in therapeutic contexts [27]. Mamatha et al. use the leaf extract of Centella asiatica, which is well-known in Indian traditional medicine for its neuroprotective properties, to create cerium oxide nanoparticles. Significant scavenging activity, improved cell viability, decreased lactate dehydrogenase and protein carbonyls, suppressed reactive oxygen species generation and apoptosis, and increased antioxidant enzyme activity are all displayed by CeO_2 nanoparticles, which raises the possibility that they could be used to treat oxygen species-related neurodegenerative diseases [28].

Using Osmium Sanctum leaf extract as a chelating and capping agent, Iqbal et al. investigate synthesis techniques and evaluate the physical characteristics of CeO_2 nanoparticles, as tiny as ~9 nm, produced using a green procedure. The typical crystallite size of CeO_2 nanoparticles produced chemically is about 17 nm. It is suggested that more research be done on these nanoparticles' possible antibacterial effectiveness against different harmful bacterial strains. This work highlights the potential of environmentally friendly synthesis techniques and highlights the adaptable characteristics of CeO_2 nanoparticles for a range of uses [29]. In order to address concerns about hypermagnesemia, Muruganandam et al. developed a very sensitive electrochemical sensor for Mg(II) ion detection. By using cerium oxide microcuboids that were created by microwaves and immobilised on a glassy carbon electrode, the sensor demonstrated remarkable electrocatalytic activity that improved the Mg(II) reduction signal. Excellent anti-interferent ability, repeatability, stability, and reproducibility were displayed by the sensor, making it appropriate for practical Mg(II) ion detecting applications [30]. The effectiveness of cerium oxide nanoparticles for the adsorptive removal of different spectral indices of natural organic matter was examined by Mahato et al. Temkin isotherms, with a maximum adsorption capacity of 238.9 mg/g (CONP-I) at neutral pH, better represented the results when operational factors and thermodynamic characteristics were examined [31].

Allu et al. explore wound healing's intricacies, noting its complexity and the influence of various cell types across different phases. Chronic wounds often arise from underlying health issues such as diabetes, hypertension, and immune deficiencies. Nanomaterials like gold, silver, cerium oxide, and zinc nanoparticles are studied for their antibacterial

properties and large surface area, beneficial for wound healing. Specifically, the review focuses on cerium oxide nanoparticles, highlighting their roles in inflammation reduction, hemostasis enhancement, proliferation stimulation, and reactive oxygen species scavenging. CeO_2 demonstrates regenerative, anti-inflammatory, and antioxidant properties that help promote wound healing, tissue regeneration, and scar reduction. They may also be advantageous in preventing bacterial infections and enhancing wound immunity. To ensure the best possible use of CeO_2 nanoparticles in wound healing, more study is necessary to completely understand their safety, effectiveness, and long-term effects on human health and the environment [32].

In the present study, the author plans to investigate the impact of probe sonication on the structural, optical, and thermal properties of CeO_2 nanoparticles. CeO_2 nanoparticles were synthesized using a novel co-precipitation method and subjected to varying sonication durations (0, 15, 30, 45, and 60 minutes). Additionally, measurements of the extinction coefficient, refractive index, optical conductivity, and both the real and imaginary components of the dielectric constant were conducted to perform a comprehensive optical study of the CeO_2 nanoparticles. This study highlights the crucial role of sonication in tailoring the properties of CeO_2 nanoparticles, offering insights for optimizing synthesis protocols for various applications requiring precise control over optical properties and particle size.

2. Experimental Section

In the present work, cerium nitrate hexahydrate, potassium carbonate and distilled water was used to prepare the CeO_2 nanoparticles procured from SD Fine, India without further purification.

CeO_2 nanoparticles were prepared via a unique method. First, 2.17 g of $Ce(NO_3)_3{\cdot}6H_2O$ was dissolved in 250 mL of distilled water to create a 0.02 M solution of Ce(III) nitrate, and 1.036 g of K_2CO_3 was dissolved in 250 mL of distilled water to create a 0.03 M solution of K_2CO_3. Then, to 100 mL of well-stirred water, drop by drop were added 50 mL of the Ce (III) nitrate solution and 20 mL of the K_2CO_3 solution. In order to precipitate cerium (III) carbonate, a white precursor, the pH had to be kept at 6 throughout this procedure. After two hours of drying at 65°C, the final product was cooled to room temperature. After that, the dry product was aged for 2.5 hours at 220°C without being cleaned or purified. Eventually, CeO_2 nanoparticles were produced by calcining the aged product for three hours at 600°C.

X-ray diffraction (XRD) was used to validate the crystal structure of the synthesised CeO_2 nanoparticles. The XRD study was done using a Rigaku Mini-Flex-II diffractometer with CuKα radiation (λ = 1.5418 Å). With a scanning rate of 0.02° s^{-1}, the scanning range was set between 10° and 90°. The CeO_2 nanoparticles' morphology was investigated by the use of scanning electron microscopy (SEM). The SEM study was done with a JEOL JSM-6300 microscope running at a voltage of 5 kV. To examine the different vibrational modes in the CeO_2 nanoparticles, Raman spectroscopy was used. Mettler Toledo React-Raman 802L spectrometer was used to gather the Raman spectra.

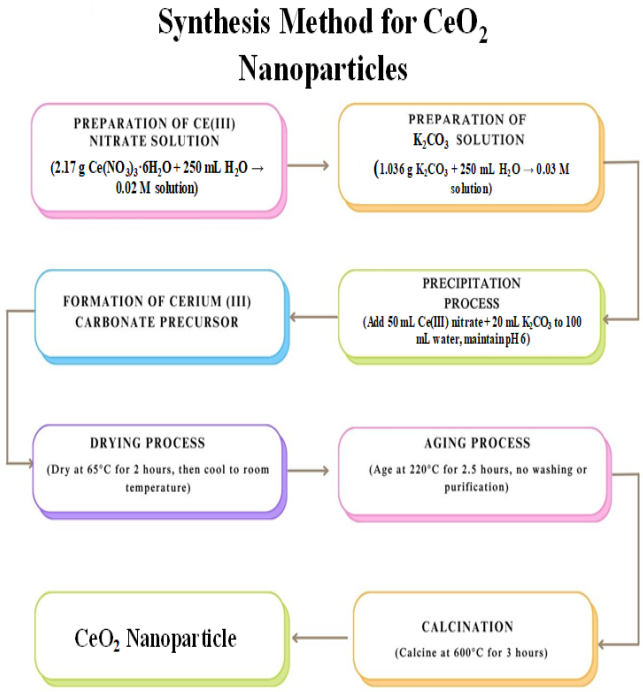

Figure 1. Pictorial representation of synthesis method for CeO_2 nanoparticles.

The optical characteristics of the CeO_2 nanoparticles were examined using ultraviolet-visible (UV-Vis) spectroscopy. Agilent Cary 60 UV-Visible Spectrometer was used to get the UV-Vis spectra. A HITACHI F-7000 Fluorescence Spectrophotometer was used to record the fluorescence spectra of the composite material. Measurements of photoluminescence (PL) spectra were also made in order to assess how particle size affected the optical characteristics. Using a Horiba Particle Size Analyser (LA-960) and doubly distilled water as the dispersion medium, the particle size distributions of the synthesised CeO_2 powders were ascertained. To evaluate the thermal stability of the nanoparticles, thermogravimetric analysis (TGA) was carried out in a nitrogen environment using a Shimadzu DTG-60h thermal analyser. By employing a probe sonication technique, the CeO_2 nanoparticles' particle size was successfully decreased. The PCI Analytics probe sonicator was utilised. Probe sonication was applied to the nanoparticles for four distinct periods of time: fifteen, thirty, forty, and sixty minutes. Their band gap and optical characteristics were also impacted by this treatment.

3. Results and Discussion

The XRD pattern of probe-sonicated CeO_2 nanoparticles over the following durations is shown in Figure 2: (a) 0 Min, (b) 15 Min, (c) 30 Min, (d) 45 Min, and (e) 60 Min. The JCPDS card number 34-0394 is used to index the peaks, which shows that the samples of CeO_2 nanoparticles have FCC structure with lattice parameters of α=β=γ= 90° and a=b=c=5.411 Å.

The creation of nanosized CeO_2 is suggested by the diffraction peaks seen at 28.56°, 33.08°, 47.47°, 56.36°, 59.08°, 69.40°, 76.70°, 79.07°, and 88.41° [33]. The fact that there are no contaminants suggests that the co-precipitation process is used to create pure CeO_2.

Using the Debye-Scherrer equation, the average crystallite size of CeO_2 nanoparticles was determined [34]. It is clear that the particle size of CeO_2 nanoparticles reduces as the probe sonication duration increases. The XRD patterns, where the peak width rises with the length of probe sonication, make this quite evident. Table 1 shows the fluctuation in particle size caused by the length of the probe sonication. The broadening of the diffraction peaks amply illustrates how the particle size decreases with increasing probe sonication time.

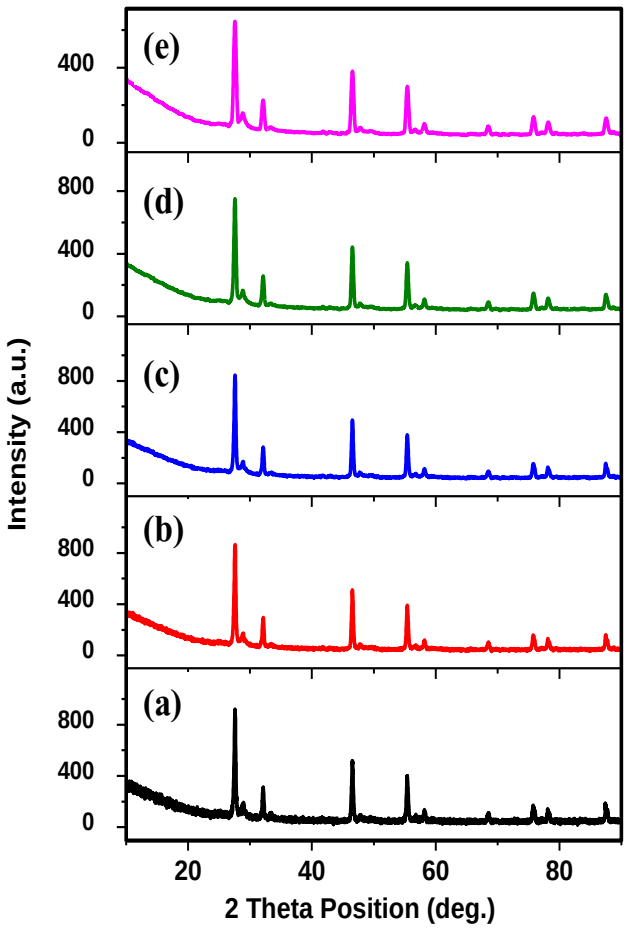

Figure 2. XRD pattern of probe sonicated CeO_2 nanoparticles for duration (a) 0 Min, (b) 15 Min, (c) 30 Min, (d) 45 Min and (e) 60 Min.

Table 1. Variation of particle size of CeO_2 nanoparticles due to probe sonication.

Probe Sonication Time (Min)	FWHM	Particle Size (nm)
0	0.28	29.2
15	0.4	20.4
30	0.44	18.6
45	0.5	16.3
60	0.56	14.6

The TEM picture of CeO_2 nanoparticles is shown in Figure 3, which unequivocally verifies that they formed as suggested. With an average diameter of 32 nm, the crystallite size estimated from XRD analysis agrees well with the average particle size shown in the TEM pictures. As can be seen in the image, individual particles have combined to produce bigger secondary particles. This is a phenomena that is also shown in the SEM image that will be discussed in a later section. The high surface energy of the nanoparticles resulting from surface charge is the cause of this aggregation. Figure 3 also displays the synthesised CeO_2 selected area electron diffraction (SAED) pattern, which attests to the nanoparticles' crystalline clarity. The production of CeO2 is supported by the SAED patterns.

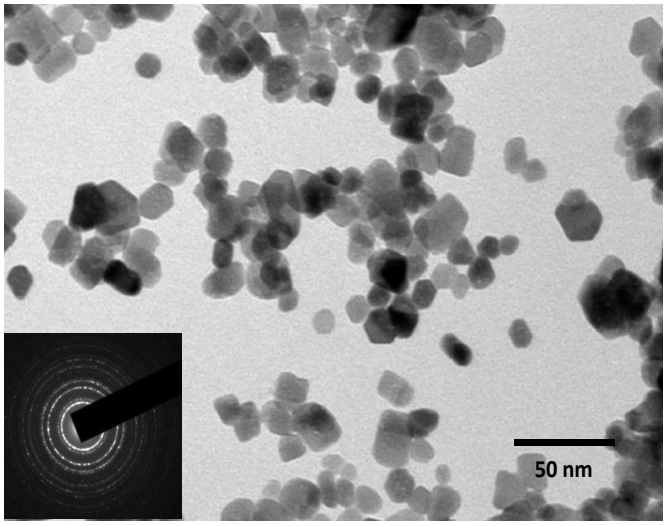

Figure 3. TEM and SAED pattern of pure CeO_2 nanoparticles.

Figure 4 (a-d) depicts the SEM micrographs of CeO_2 nanoparticles probe sonicated for various duration 15 min, 30 min, 45 min and 60 min, respectively. Figure 4(a) depicts the SEM image of CeO_2 nanoparticles sonicated for 15 minutes shows a relatively irregular and aggregated structure. The nanoparticles appear to be loosely packed, with varying sizes and shapes. Some clusters are evident, indicating incomplete dispersion at this stage. After 30 minutes of sonication as shown in Figure 4(b), the SEM image reveals a more uniform distribution of CeO_2 nanoparticles. The particles are more distinct and begin to exhibit a more spherical morphology. Aggregation is reduced compared to the 15-minute sample, and the size distribution appears narrower, indicating improved dispersion. The SEM image (Figure 4-c and d) of CeO_2 nanoparticles sonicated for 45 and 60 minutes, respectively shows further improvement in dispersion and uniformity. The nanoparticles are well-defined and exhibit a more consistent spherical shape. The particle size appears more uniform, and there is a significant reduction in aggregation, suggesting effective sonication at this duration. It is observed that probe sonication process significantly reduces the particle size.

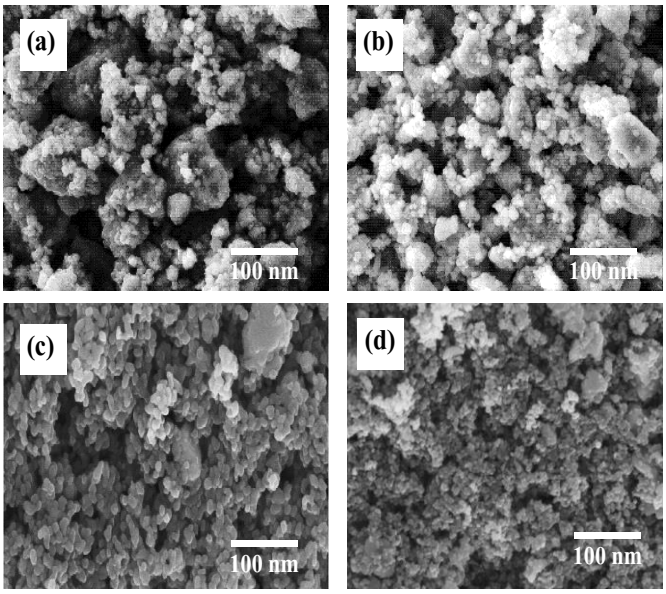

Figure 4. SEM images of CeO_2 nanoparticles probe sonicated for the duration (a) 15 Min, (b) 30 Min, (c) 45 Min and (d) 60 Min.

Figure 5 (a-d) displays the Raman spectra of CeO_2 nanoparticles that were sonicated for 15, 30, 45, and 60 minutes. CeO_2 is a member of the O5h (Fm3m) space group and has a fluorite structure that is cubic. The first-order Raman line at around 465 cm^{-1}, which is attributed to the triply degenerate Raman active optical phonon mode (F2g), is the main Raman characteristic that is detected. This distinctive peak identifies the fluorite phase of CeO_2.

The peak positions of the Raman bands expand, move to lower energy, and become more asymmetric as the particle size decreases. The vibrational characteristics of smaller nanoparticles are affected by phonon confinement and an increased surface-to-volume ratio, which is the reason for this phenomenon [35].

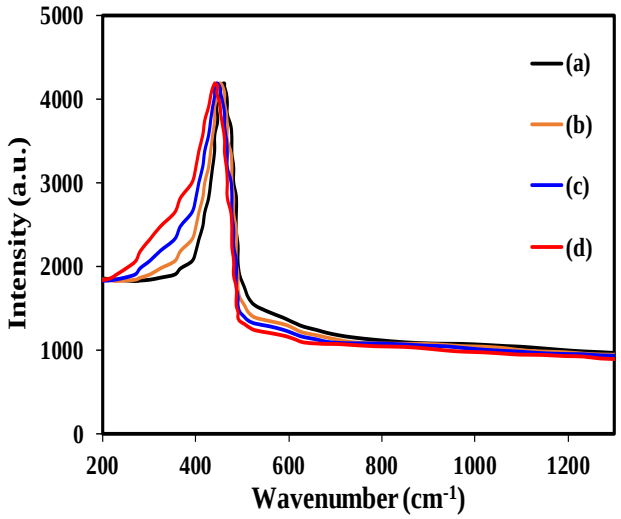

Figure 5. Raman spectra of CeO_2 nanoparticles probe sonicated for the duration (a) 15 Min, (b) 30 Min, (c) 45 Min and (d) 60 Min.

UV-Vis absorption spectra of CeO_2 nanoparticles that were sonicated for several lengths of time—15, 30, 45, and 60 minutes—are displayed in Figure 6. To comprehend the impact of sonication duration on particle size, the optical characteristics of the nanoparticles were examined. Particle size decreases with increasing probe sonication time. This tendency is demonstrated by the shift in the absorption edge to shorter wavelengths (blue shift) with increasing sonication duration, a behaviour often linked with the quantum confinement effect in nanoparticles [36]. The gradual blue shift of the absorption edge in the UV-Vis spectra in Figure 6 shows a definite trend of decreasing particle size with increasing sonication duration. This change is explained by the quantum confinement phenomenon, which causes absorption at shorter wavelengths when smaller nanoparticles have greater bandgap energies. The results of the Raman and SEM spectroscopy are supported by the UV-Vis analysis, which emphasises how well probe sonication works to regulate the particle size of CeO_2 nanoparticles [37].

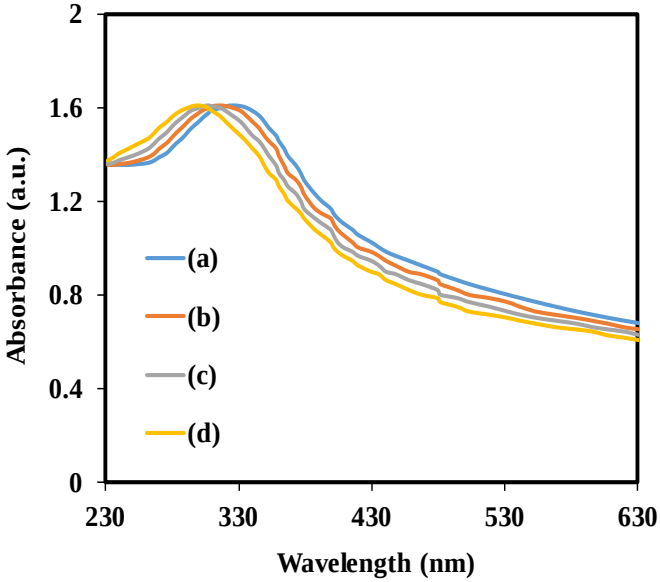

Figure 6. UV-Vis spectra of CeO_2 nanoparticles probe sonicated for the duration (a) 15 Min, (b) 30 Min, (c) 45 Min and (d) 60 Min.

The photoluminescence (PL) spectra of CeO_2 nanoparticles sonicated for several lengths of time, namely 15 minutes, 30 minutes, 45 minutes, and 60 minutes, are displayed in Figure 7. To learn more about the optical emission characteristics of the nanoparticles and how sonication duration affects them, PL measurements were performed at an excitation wavelength of 350 nm. After 15 minutes of sonication, the CeO_2 nanoparticle PL spectrum shows a large emission peak in the visible region. Recombination of electrons and holes in defect states, including oxygen vacancies, which are common in CeO_2 nanoparticles, is the main cause of this emission. The PL peak comparatively high intensity suggests that defect states that promote radiative recombination are significantly present [38].

The PL spectra for the 30-minute sonicated sample reveals a drop in emission intensity when compared to the 15-minute sample. This drop in intensity points to a reduction in the number of defect states and an improvement in the nanoparticles' crystalline quality. A decrease in particle size is

shown by the emission peak's faint blue shift. Further sonication for 45 minutes results in a more pronounced decrease in PL emission intensity. The emission peak continues to shift slightly towards the blue region, consistent with a further reduction in particle size and defect density. The decreased intensity reflects fewer radiative recombination centers due to improved crystallinity. The PL spectrum for the 60-minute sonicated sample displays the lowest emission intensity among all the samples. This significant decrease in PL intensity indicates the smallest particle size and the lowest defect density achieved with the longest sonication duration. The blue shift of the emission peak is more pronounced, highlighting the quantum confinement effect in smaller nanoparticles [39].

The effect of sonication period on the optical emission characteristics of CeO_2 nanoparticles is shown by the PL spectra in Figure 7. The emission peak shifts to the blue and the intensity of photoluminescence drops as the sonication time increases due to a decrease in particle size. Longer sonication reduces defect states and improves crystalline quality, which leads to fewer radiative recombination centres, which is the reason for this trend. The PL analysis results are consistent with the results obtained from Raman, SEM, and UV-Vis spectroscopy, highlighting the usefulness of probe sonication in improving the optical and structural characteristics of CeO_2 nanoparticles.

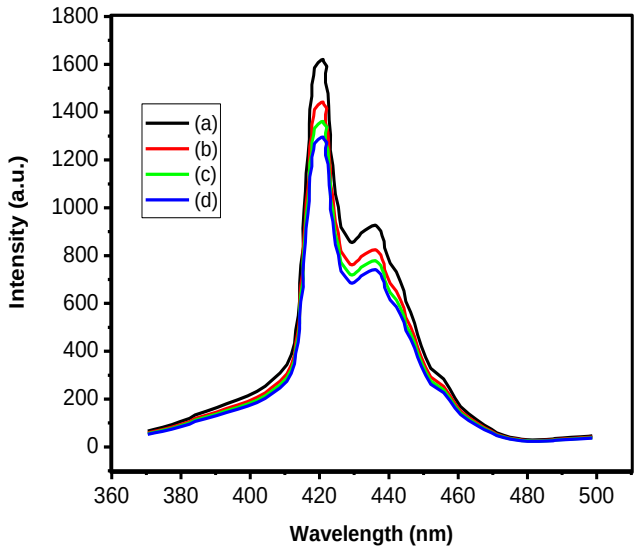

Figure 7. PL spectra of CeO_2 nanoparticles probe sonicated for the duration (a) 15 Min, (b) 30 Min, (c) 45 Min and (d) 60 Min.

Figure 8 illustrates the dynamic light scattering (DLS) analysis of CeO_2 nanoparticles subjected to varying sonication durations: (a) 15 minutes, (b) 30 minutes, (c) 45 minutes, and (d) 60 minutes. The DLS results indicate distinct particle size distribution peaks corresponding to each duration: 21.2 nm for 15 minutes, 18.3 nm for 30 minutes, 16.8 nm for 45 minutes, and 15.2 nm for 60 minutes. As sonication time increases, there is a clear trend of decreasing average particle size and narrowing size distribution. The initial 15-minute sonication shows larger particle sizes with some agglomeration, gradually reducing with longer sonication durations. The 60-minute sample exhibits the smallest and most uniformly dispersed nanoparticles, indicating effective dispersion and minimal agglomeration [40]. These findings corroborate with other analytical techniques such as UV-Vis, SEM, Raman, and PL spectroscopy, highlighting the role of prolonged sonication in enhancing the uniformity and size control of CeO_2 nanoparticles.

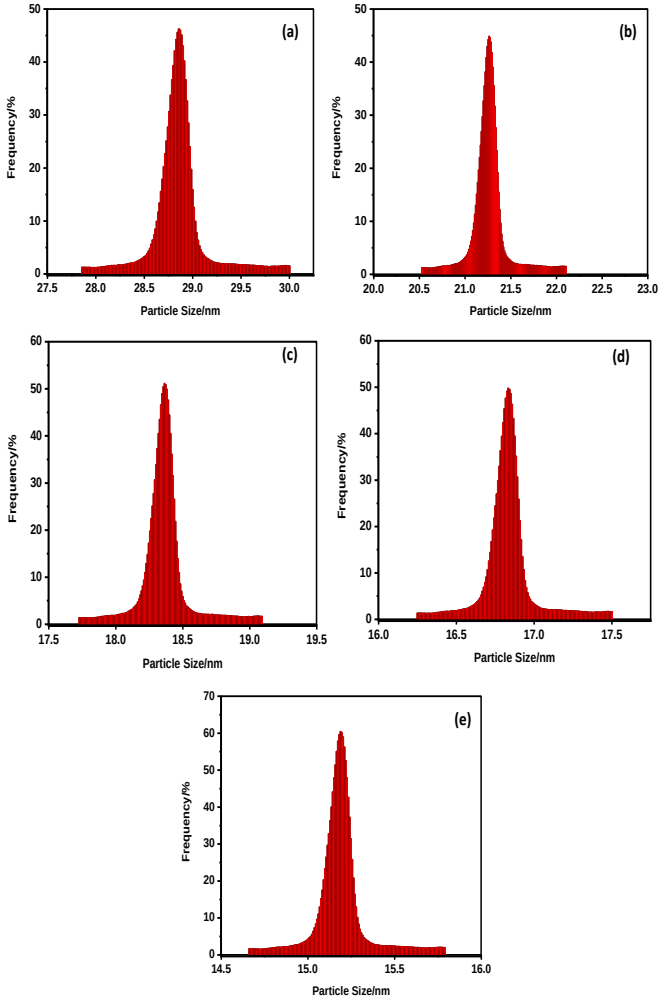

Figure 8. DLS analysis of the particle size distribution of CeO_2 nanoparticles probe sonicated for the duration (a) 15 Min, (b) 30 Min, (c) 45 Min and (d) 60 Min.

The thermogravimetric (TG) and differential thermal analysis (DTA) results for probe-sonicated CeO_2 nanoparticles and pure CeO_2 are displayed in Figure 9(a-b). In TG analysis, pure CeO_2 nanoparticles show discrete weight loss phases. The dehydration of CeO2·H2O to CeO_2 is responsible for the first 16.0% drop in weight loss at 120°C. The DTA curve shows an endothermic peak at 117°C in conjunction with this. The breakdown of leftover nitrates and oxygen loss combustion are indicated by subsequent weight losses of 8% at 300°C, with an exothermic peak at 313°C, and 4% at 800°C, corresponding to an exothermic peak at 813°C, respectively. In contrast, probe sonicated CeO_2 nanoparticles, treated for 60 minutes, likely show altered TG and DTA profiles due to reduced particle sizes from improved dispersion and reduced agglomeration. Sonication enhances

surface area, potentially accelerating initial decomposition kinetics and altering peak temperatures in DTA analysis. These changes reflect the influence of particle size on thermal stability, suggesting that smaller particles may exhibit earlier onset of decomposition and modified thermal behavior compared to their larger counterparts. Understanding these differences is crucial for tailoring CeO_2 nanoparticles for applications requiring precise thermal properties and stability [41].

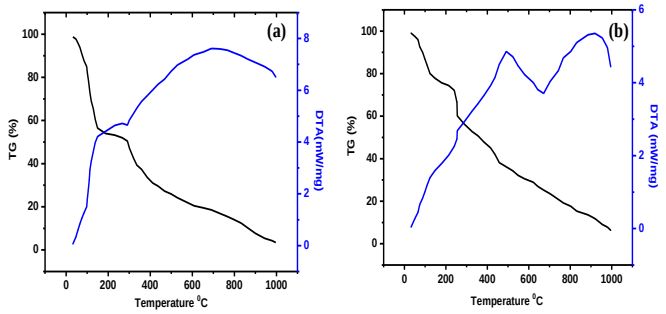

Figure 9. TG-DTA analysis of (a) CeO_2 nanoparticles and CeO_2 nanoparticles probe sonicated for 60 Min.

Figure 10 illustrates a consistent decrease in the optical band gap of CeO_2 nanoparticles with an increase in probe sonication time. Table 2 shows that after 15 minutes of sonication, the absorption wavelength changes to 411.90 nm from 441.22 nm. The optical band gap correspondingly narrows, reaching 3.01 eV after 60 minutes from 2.81 eV at 15 minutes. This pattern indicates that extended sonication increases the CeO_2 nanoparticles crystallinity and decreases their particle size, which causes the absorption edge to move blue and the optical band gap to widen. The reduction in band gap indicates an improvement in the electronic properties, potentially making these nanoparticles more suitable for applications requiring specific optical characteristics, such as photocatalysis or optical sensors. Understanding these variations is crucial for optimizing the synthesis conditions of CeO_2 nanoparticles based on desired optical properties.

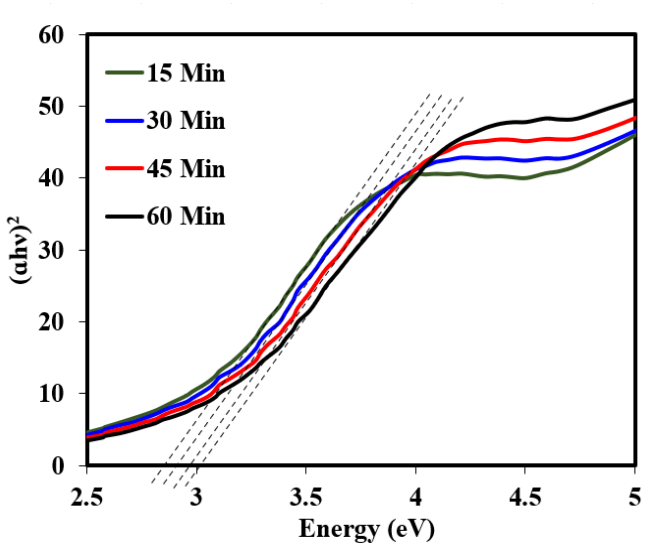

Figure 10. Optical band gap spectra of CeO_2 nanoparticles probe sonicated for the duration (a) 15 Min, (b) 30 Min, (c) 45 Min and (d) 60 Min.

Table 2. Variation of optical band gap of CeO_2 nanoparticles due to probe sonication.

Probe Sonication Time (Min)	Absorption Wavelength (nm)	Optical Band Gap (eV)
15	441.22	2.81
30	429.01	2.89
45	418.86	2.96
60	411.90	3.01

Figure 11 illustrates how the extinction coefficient changes with wavelength. The percentage of light lost as a result of scattering and absorption per unit distance of the penetrating medium is measured by the extinction coefficient (K). In other words, it's the wave energy that is lost to the substance. It is calculated in the sample utilising the connection between wavelength and percent absorption while it is exposed to UV spectrum. Equation 1 [42] provides the extinction coefficient (K):

$$K=\frac{\alpha\lambda}{4\pi} \quad (1)$$

where α is the % absorption and λ is the wavelength. The extinction coefficient spectra of CeO_2 nanoparticles probe sonicated for durations of 15 min, 30 min, 45 min, and 60 min show that the extinction coefficient gradually increases between 250 nm and 320 nm for all samples. It is further clearly observed that the magnitude of extinction coefficient decreases with increasing probe sonication time. The relationship between probe sonication time and both the particle size and extinction coefficient of CeO_2 nanoparticles shows that both parameters decrease with increasing sonication time. The extinction coefficient is influenced by the size, shape, and concentration of nanoparticles. Smaller particles have different light interaction properties compared to larger particles. As sonication reduces particle size, the manner in which the nanoparticles absorb and scatter light changes. Smaller particles generally scatter light less effectively than larger particles, leading to a reduction in the extinction coefficient.

Smaller nanoparticles have a higher surface area-to-volume ratio, which can influence how they interact with light. The increased surface area can lead to more efficient light absorption, but the overall energy loss per particle decreases as the size reduces. Understanding the relationship between sonication time, particle size, and extinction coefficient allows for the design of nanoparticles with desired properties for enhanced performance in various applications. In summary, increasing probe sonication time reduces the particle size of CeO_2 nanoparticles, which in turn decreases their extinction coefficient. This relationship is crucial for manipulating the optical and physical properties of CeO_2 nanoparticles for specific applications.

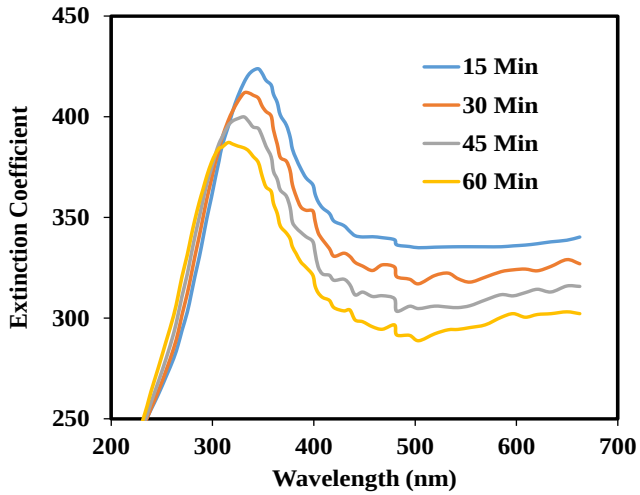

Figure 11. Extinction Coefficient spectra of CeO_2 nanoparticles probe sonicated for the duration 15 Min, 30 Min, 45 Min and 60 Min.

The Refractive Index and Optical Conductivity spectra of CeO_2 nanoparticles probe-sonicated for 15, 30, 45, and 60 minutes are displayed in Figure 12. The optical reaction of a material is mainly studied in terms of the optical conductivity (σ), which is given by the relation (Equation 2) [43]:

$$\sigma = \frac{\alpha h\upsilon}{4\pi} \quad (2)$$

where α is the absorption coefficient, n is the refractive index, c is the velocity of light, and hυ represents the photon energy. Both the refractive index and optical conductivity spectra gradually increase between 350 nm and 450 nm versus wavelength for all probe-sonicated samples. In both cases, it is observed that the magnitude of the refractive index and optical conductivity spectra is influenced by probe sonication time, which is due to changes in particle size.
The refractive index (n) of a material is a measure of how much the speed of light is reduced inside the material. It is influenced by the electronic structure and the density of the material.

As the particle size decreases with increased sonication time, the density of electronic states may change, leading to variations in the refractive index. Smaller particles can cause more uniform distribution in the medium, which can influence the refractive index. Nanoparticles have a high surface area-to-volume ratio. As grain size reduces, surface effects become more pronounced, affecting the refractive index. The increased surface area can alter the electronic polarizability, thereby changing the refractive index.

Optical conductivity (σ) represents how well a material can conduct light-induced electric currents. It is related to the absorption coefficient (α), which is influenced by particle size: Smaller nanoparticles have a higher absorption coefficient due to the increased surface area and altered electronic structure. This leads to more efficient absorption of photon energy, thereby increasing the optical conductivity.

As the sonication time increases, the resulting smaller particles have more surface states, which can enhance the interaction with light and improve optical conductivity. However, beyond 450 nm, the decrease in optical conductivity indicates that the material's ability to absorb and conduct light energy diminishes at these longer wavelengths.

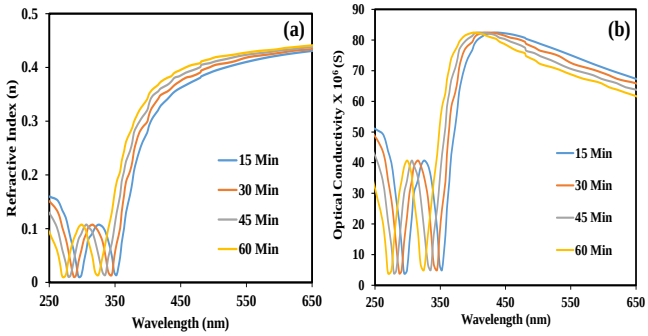

Figure 12. (a) Refractive Index spectra and (b) Optical Conductivity Spectra of CeO_2 nanoparticles probe sonicated for the duration 15 Min, 30 Min, 45 Min and 60 Min.

Among the essential characteristics of the substance is its actual and imagined dielectric constant. Equations 3 and 4, respectively, can be used to estimate the real and imaginary components of the dielectric constant [44],

$$\varepsilon_r = n^2 - K^2 \quad (3)$$

$$\varepsilon_i = 2nK \quad (4)$$

The dielectric constant actual function is to calculate how much a substance will slow down light in that material. The actual dielectric constant fluctuation as a function of photon energy is seen in Figure 13. Figure 9 illustrates the fluctuation of the imaginary dielectric constant as a function of photon energy, whereas the section on the imaginary dielectric constant demonstrates how a dielectric material absorbs energy from an electric field owing to dipole motion.

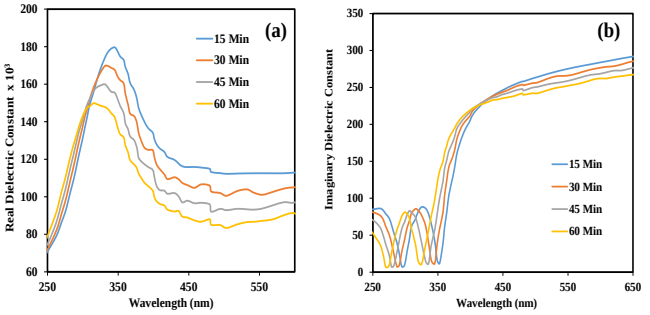

Figure 13. (a) Real Dielectric Constant and (b) Imaginary Dielectric Constant of CeO_2 nanoparticles probe sonicated for the duration 15 Min, 30 Min, 45 Min and 60 Min.

4. Conclusions and Future Scope

Probe sonication significantly influences the physical properties of CeO_2 nanoparticles. Extended sonication times lead to smaller, more uniform nanoparticles with enhanced optical and thermal characteristics. These findings underscore the importance of sonication in tailoring the properties of CeO_2 nanoparticles for potential applications in

photocatalysis, optical sensors, and other areas requiring precise control of nanoparticle properties. The study provides a comprehensive understanding of how sonication time affects CeO_2 nanoparticles, offering insights for optimizing synthesis protocols for specific applications. The future scope of this work includes exploring the potential applications of cerium oxide nanoparticles in environmental remediation, energy storage, and catalytic processes.

Structural and Morphological Properties:

- XRD analysis confirmed the formation of pure, face-centered cubic structured CeO_2 nanoparticles, with a notable reduction in particle size as the sonication time increased. The particle size decreased from 29.2 nm (no sonication) to 14.6 nm (60 minutes of sonication).
- TEM and SEM images corroborated the XRD findings, showing reduced particle aggregation and improved uniformity with longer sonication times.

Optical Properties:

- UV-Vis analysis revealed a blue shift in the absorption edge, indicative of the quantum confinement effect, with increasing sonication time. The optical band gap raises from 2.81 eV (15 minutes) to 3.01 eV (60 minutes).
- PL spectroscopy demonstrated a decrease in emission intensity and a blue shift in the emission peak with prolonged sonication, suggesting improved crystalline quality and reduced defect density.
- The optical properties were found to be influenced by the sonication duration, showing a decrease in particle size and enhanced uniformity leading to changes in these optical parameters.

Thermal Properties:

- TG-DTA analysis indicated distinct weight loss steps associated with dehydration and decomposition processes.
- Sonicated samples exhibited altered thermal behavior due to reduced particle sizes and enhanced dispersion.

Complex Optical Study:

- The extinction coefficient and refractive index spectra showed a gradual increase between 250 nm and 320 nm, with magnitudes decreasing with longer sonication times, indicating effective reduction in particle size and improved dispersion.
- The optical conductivity exhibited an increase up to 450 nm, followed by a decrease beyond this wavelength, highlighting the changes in particle size and interaction with light due to extended sonication.

Conflict of Interest

Authors declare that they do not have any conflict of interest.

Funding Source

No funding was received for this research work.

Authors' Contributions

Author-1 reviewed literature and identified the problem of study and wrote the first draft of the manuscript.

Author-2 involved in solving equation and plotting graph using software. Also approved the final version of the manuscript.

Author-3 reviewed and edited the manuscript and approved the final version of the manuscript.

Acknowledgements

The authors gratefully acknowledge the support and necessary academic assistance provided by the Principal, Arts, Science and Commerce College, Chikhaldara- 444807, Maharashtra, India.

References

[1] K.R.B. Singh, V. Nayak, T. Sarkar, R. Pratap, "Cerium oxide nanoparticles: properties, biosynthesis and biomedical application," *RSC Advances*, Vol.**10**, Issue. **27194**, pp.**27194–27214, 2020.**

[2] M. Guo, C. Guo, L. Jin, Y. Wang, "Nano-sized CeO2 with extra-high surface area and its activity for CO oxidation," *Materials Letters*, Vol.**64**, Issue.**1638**, pp.**1638-1640, 2010**.

[3] K. Hudda, B. Rathee, M. Wati, S. Ranga, R. Tyagi, "Some Applications of CeO_2 Nanoparticles," *Oriental Journal of Chemistry*, Vol. **39**, Issue. **684**, pp. **684-693, 2023**.

[4] T.S. Cam, S.O. Omarov, M.I. Chebanenko, S.G. Izotova, V.I. Popkov, "Recent progress in the synthesis of CeO2-based nanocatalysts towards efficient oxidation of CO," *Journal of Science: Advanced Materials and Devices*, Vol.**7**, Issue.**100399**, pp.**100399, 2022**.

[5] N. Radic, B. Grbic, S. Petrovic, S. Stojadinovic, N. Tadic, P. Stefanov, "Effect of cerium oxide doping on the photocatalytic properties of rutile TiO_2 films prepared by spray pyrolysis," *Physica B: Condensed Matter*, Vol. **599**, Issue. **412544**, pp. **412544, 2020**.

[6] W. Wang, B. Zhang, S. Jiang, H. Bai, S. Zhang, "Use of CeO_2 nanoparticles to enhance UV-shielding of transparent regenerated cellulose films," *Polymers*, Vol.**11**, Issue.**48**, pp.**458, 2019.**

[7] A. Morlando, M. Borras, Y. Rehman, S. Bakand, P. Barker, R. Sluyter, K. Konstantinov, "Development of CeO_2 nanodot encrusted TiO_2 nanoparticles with reduced photocatalytic activity and increased biocompatibility towards a human keratinocyte cell line," *Journal of Materials Chemistry B*, Vol.**8**, Issue.**16**, pp.**4016-4028, 2020**.

[8] R.F.S. Mariana, F.R.P. Alves Manuel, P.G.Q. Cunha Joao, L. Costa, A.S. Cristina, M.H.V. Fernandes, P.M. Vilarinho, P. Ferreira, "Nanostructured transparent solutions for UV-shielding: Recent developments and future challenges," *Materials Today Physics*, Vol.**35**, Issue. **23**, pp.**101131**, **2023.**

[9] M. Khan, Z. Mashwani, M. Ikram, N.I. Raja, A.H. Mohamed, G. Ren, A.A. Omar, "Efficacy of green cerium oxide nanoparticles for potential therapeutic applications: Circumstantial Insight on Mechanistic Aspects," *Nanomaterials*, Vol.**12**, Issue. **2, pp.2117, 2022.**

[10] A.S. Fudala, W.M. Salih, F.F. Alkazaz, "Synthesis of different sizes of cerium oxide (CeO_2) nanoparticles by using different concentrations of precursor via sol–gel method," *Materials Today: Proceedings*, Vol.**49**, Issue. **8**, pp.**2786-2792, 2022**.

[11] D.N. Oosthuizen, D.E. Motaung, H.C. Swart, "Gas sensors based on CeO_2 nanoparticles prepared by chemical precipitation method and their temperature-dependent selectivity towards H_2S and NO_2 gases," *Applied Surface Science*, Vol.**505**, Issue.**14, pp.144356, 2020.**

[12] L.D. Sonawane, A.S. Mandawade, L.N. Bhoye, H.I. Ahemad, S.S. Tayade, Y.B. Aher, A.B. Gite, L.K. Nikam, S.D. Shinde, G.H. Jain, G.E. Patil, M.S. Shinde, "Sol-gel and hydrothermal synthesis of CeO_2 NPs: Their physiochemical properties and applications for gas sensor with photocatalytic activities," *Inorganic Chemistry Communications*, Vol.**164**, Issue.**112313, pp.112313, 2024.**

[13] T.M. Nimbalkar, Y.M. Jadhav, R.N. Dhanawade, N.S. Pawar, A.C. Molane, S.S. Gavande, G.T. Chavan, C. Jeon, S.D. Sartale, V.B. Patil, "Simple chemical synthesis of CeO_2 nanoparticles for toxic NO_2 gas detection," *Journal of Alloys and Compounds*, Vol.**966**, Issue.**171461**, pp.**171461, 2023**.

[14] V. Pathak, P. Lad, A.B. Thakkar, P. Thakor, M.P. Deshpande, S. Pandya, "Synthesis, characterization and applications of cubic fluorite cerium oxide nanoparticles: A comprehensive study," *Results in Surfaces and Interfaces*, Vol.**11**, Issue.**14, pp.100111, 2023.**

[15] A.A. Kabure, B.S. Shirke, S.R. Mane, K.M. Garadkar, "Microwave-assisted sol-gel synthesis of CeO_2–NiO nanocomposite based NO_2 gas sensor for selective detection at lower operating temperature," *Journal of the Indian Chemical Society*, Vol.**99**, Issue.**36**, pp.**100369, 2022.**

[16] M.S. Pujar, S.M. Hunagund, D.A. Barretto, "Synthesis of cerium-oxide NPs and their surface morphology effect on biological activities," *Bulletin of Materials Science*, Vol.**43**, Issue.**14**, pp.**26-38, 2020.**

[17] H. Ko, G. Yang, H. Cheng, M. Wang, X. Zhao, "Growth and optical properties of cerium dioxide nanocrystallites prepared by coprecipitation routes," *Ceramics International*, Vol.**40**, Issue. **55**, pp.**4055-4064, 2014**.

[18] D.K. Kumar, P. Bharathi, A. Govind, J. Archana, M. Navaneethan, S. Harish, "Detection of NO_2 at ppm-level using Al-doped CeO_2 based gas sensor with high sensitivity and selectivity at room temperature," *Journal of Environmental Chemical Engineering*, Vol.**12**, Issue.**16**, pp.**112253, 2024.**

[19] C. Liu, H. Tai, P. Zhang, Z. Yuan, X. Du, G. Xie, Y. Jiang, "A high-performance flexible gas sensor based on self-assembled PANI-CeO_2 nanocomposite thin film for trace-level NH_3 detection at room temperature," *Sensors and Actuators B*, Vol. **261**, Issue. **268**, pp. **2017261, 2017**.

[20] M. Li, W. Ren, R. Wu, M. Zhang, "CeO2 Enhanced Ethanol Sensing Performance in a CdS Gas Sensor," *Sensors*, Vol.**17**, Issue.**1577**, pp.**1577, 2017**.

[21] D. Mohanta, S.V. Gupta, V. Gadore, S. Paul, M. Ahmaruzzaman, "SnO_2 Nanoparticles-CeO_2 Nanorods Enriched with Oxygen Vacancies for Bifunctional Sensing Performances toward Toxic CO Gas and Arsenate Ions," *ACS Omega*, Vol.**7**, pp.**20357-20368**, **2022**.

[22] D. Majumder, S. Roy, "Development of Low-ppm CO Sensors Using Pristine CeO_2 Nanospheres with High Surface Area," *ACS Omega*, Vol.**3**, pp.**4433-4440**, **2018**.

[23] P.P. Tumkur, N.K. Gunasekaran, B.R. Lamani, N. Nazario Bayon, K. Prabhakaran, J.C. Hall, G.T. Ramesh, "Cerium Oxide Nanoparticles: Synthesis and Characterization for Biosafe Applications," *Nanomanufacturing*, Vol.**1**, pp.**176-189**, **2021**.

[24] J. Calvache-Munoz, F.A. Prado, J.E. Rodriguez-Paez, "Cerium Oxide Nanoparticles: Synthesis, Characterization and Tentative Mechanism of Particle Formation," *Colloids and Surfaces A: Physicochemical and Engineering Aspects*, Vol.**529**, pp.**146-159**, **2017.**

[25] R.N. Pol, K. Ashwini, "Cerium Oxide Nanoparticles: Synthesis, Characterization and Study of Antimicrobial Activity," *Journal of Nanomaterials & Molecular Nanotechnology*, Vol.**6**, Issue.**3**, pp.**37-45**, **2017**.

[26] M.E. Ioannou, G.K. Pouroutzidou, I. Chatzimentor, I. Tsamesidis, N. Florini, I. Tsiaoussis, E. Lymperaki, P. Komninou, E. Kontonasaki, "Synthesis and Characterization of Cerium Oxide Nanoparticles: Effect of Cerium Precursor to Gelatin Ratio," *Applied Sciences*, Vol.**13**, pp.**2676, 2023**.

[27] M. Nyoka, Y.E. Choonara, P. Kumar, P.P.D. Kondiah, V. Pillay, "Synthesis of Cerium Oxide Nanoparticles Using Various Methods: Implications for Biomedical Applications," *Nanomaterials*, Vol.**10**, Issue.**2**, pp.**242, 2020**.

[28] M.G. Mamatha, M.A. Ansari, M.Y. Begum, D. Prasad B., A. Al Fatease, U. Hani, M.N. Alomary, S. Sultana, S.M. Punekar, N. M.B., T.R. Lakshmeesha, T. Ravikiran, "Green Synthesis of Cerium Oxide Nanoparticles, Characterization, and Their Neuroprotective Effect on Hydrogen Peroxide-Induced Oxidative Injury in Human Neuroblastoma (SH-SY5Y) Cell Line," *ACS Omega*, Vol.**9**, Issue.**2**, pp.**2639-2649**, **2024**.

[29] A. Iqbal, A.S. Ahmed, "Comparative Study of Chemically and Green Synthesized Cerium Oxide Nanoparticles and Its Characterization," *AIP Conference Proceedings*, Vol.**2752**, pp.**040004**, **2023**.

[30] G. Muruganandam, N. Nesakumar, A. Jayalatha, J.B.B. Rayappan, B. Mahendran, "Fabrication of Electrochemical Sensor for the Detection of Mg(II) Ions Using CeO_2 Microcuboids as an Efficient Electrocatalyst," *Chemosensors*, Vol.**11**, Issue.**8**, pp.**442, 2024.**

[31] J.K. Mahato, S.K. Gupta, "Exceptional adsorption of different spectral indices of natural organic matter (NOM) by using cerium oxide nanoparticles (CONPs)," *Environmental Science and Pollution Research*, Vol.**28**, **2021**, pp.**2021-28.**

[32] A. Allu, A.K. Sahi, P. Kumari, K. Sakhile, A. Sionkowska, S. Gundu, "A brief review on cerium oxide-based scaffolds: Recent advances in wound healing applications," *Micromachines*, Vol.**14**, **2023**, pp.**865**.

[33] M. Ansari, M. Alam, "Nickle-ion-substituted ceria nanoparticles-based electrochemical sensor for sensitive detection of thiourea," *Journal of Materials Science: Materials in Electronics*, Vol.**32**, **2021**, pp.**1-9**.

[34] K.R. Nemade, S.A. Waghuley, "Low temperature synthesis of semiconducting α-Al_2O_3 quantum dots," *Ceramics International*, Vol.**40**, **2014**, pp.**6109–6113**.

[35] R. Zamiri, H.A. Ahangar, A. Kaushal, A. Zakaria, G. Zamiri, D. Tobaldi, J.M.F. Ferreira, "Dielectrical Properties of CeO_2 Nanoparticles at Different Temperatures," *PLoS ONE*, Vol.**10**, pp.**1-11, 2015.**

[36] S. Sagadevan, M.R. Johan, A. Lett, "Fabrication of reduced graphene oxide/CeO_2 nanocomposite for enhanced electrochemical performance," *Applied Physics A*, Vol.**125**, **2019,** pp.**08-17**.

[37] L. Nurhasanah, W. Safitri, Z. Arifin, A. Subagio, "Antioxidant activity and dose enhancement factor of CeO2 nanoparticles synthesized by precipitation method," *IOP Conference Series Materials Science and Engineering*, Vol.**432**, **2018**, pp.**012031**.

[38] M.A. Farrukh, K.M. Butt, K.-K. Chong, W.S. Chang, "Photoluminescence emission behavior on the reduced band gap of Fe doping in CeO2-SiO2 nanocomposite and photophysical properties," *Journal of Saudi Chemical Society*, Vol.**23**, **2019**, pp.**561-575**.

[39] F. Sanhueza, E. Valdebenito, R. Udayabhaskar, C. Salvo, S.F. Sahlevani, E. Elgueta, M. Parra, H. Bello, R.V. Mangalaraja, "Effect of ultrasonic sonication time on the structural, optical and antibacterial properties of ceria nanostructures," *Materials Research Express*, Vol.**6**, **2019**, pp.**095055**.

[40] J. Hou, H. Ci, P. Wang, C. Wang, B. Lv, L. Miao, G. You, "Nanoparticle tracking analysis versus dynamic light scattering: Case study on the effect of Ca^{2+} and alginate on the aggregation of cerium oxide nanoparticles," *Journal of Hazardous Materials*, Vol.**360**, **2018**, pp.**319-328**.

[41] V. Ramasamy, G. Vijayalakshmi, "Synthesis, characterization and tuning of visible region absorption ability of cadmium doped ceria quantum dots," *Journal of Materials Science: Materials in Electronics*, Vol.**27**, **2016**, pp.**4723–4735**.

[42] K.R. Nemade, S.A. Waghuley, "Synthesis of MgO Nanoparticles by Solvent Mixed Spray Pyrolysis Technique for Optical Investigation," *International Journal of Metals*, Vol. **2014**, pp.**1-4**, **2014**.

[43] P. Sharma, S.C. Katyal, "Determination of optical parameters of a-$(As_2Se_3)_{90}Ge_{10}$ thin film," *Journal of Physics D: Applied Physics*, Vol.**40**, pp.**2115–2120**, **2007**.

[44] N.A. Bakr, A.M. Funde, V.S. Waman, "Determination of the optical parameters of a-Si:H thin films deposited by hot wire–chemical vapour deposition technique using transmission spectrum only," *Pramana: Journal of Physics*, Vol.**76**, pp.**519–531, 2011**.

AUTHORS PROFILE

Mr. Shubham Kadam, Assistant Professor of Applied Physics at Prof. Ram Meghe College of Engineering and Management, Amravati, Maharashtra, has been serving in the Department of Physics since 2012. He earned his M.Sc. in Physics in 2009 from the Government Vidarbha Institute of Science and Humanities, Amravati. Over his academic career, he has published three research papers, showcasing his dedication to advancing knowledge in his field.

Dr. Vivek Dalpatrao Kapse is a distinguished academician and researcher in the field of physics. He holds an M.Sc., B.Ed., M.Phil., and Ph.D. in Physics. Currently serving as a Professor in the Department of Physics at Arts, Science, and Commerce College, Chikhaldara, Dr. Kapse has made significant contributions to scientific research, with 45 research papers published in reputed journals.

Dr. Kailash Nemade, Head and Assistant Professor at Indira Mahavidyalaya, Kalamb, Dist. Yavatmal, holds a Ph.D. from Sant Gadge Baba Amravati University, Amravati. With a distinguished academic career, he has published 82 research papers and authored 5 books in the fields of spintronics, supercapacitors, and photovoltaics. His contributions to innovation are further highlighted by a granted patent.

